POLISH JOURNAL *of* RADIOLOGY

Original paper

Correlation of texture feature analysis with bone marrow infiltration in initial staging of patients with lymphoma using 18F-fluorodeoxyglucose positron emission tomography combined with computed tomography

Mahmoud A. Kenawy[1A,B,C,D,E,F,G], Magdy M. Khalil[2A,C,D], Mahmoud H. Abdelgawad[1A], H. H. El-Bahnasawy[1A]

[1]Biophysics Branch, Department of Physics, Faculty of Science, Al-Azhar University, Nasr City, Cairo, Egypt
[2]Department of Physics, Faculty of Science, Helwan University, Cairo, Egypt

Abstract

Purpose: To explore whether radiomic features of fluorine-18-fluorodeoxyglucose (18F-FDG) positron emission tomography–computed tomography (PET/CT) has association with bone marrow infiltration (BMI) in comparison to other conventional PET metrics.

Material and methods: Forty-four patients (with pathologically proven lymphoma disease) underwent staging 18F-FDG PET/CT scan. Primary tumour was semi-automatically or manually segmented with a threshold standardised uptake value (SUV) of 3. A total of 73 features were extracted from eight different textures. Spearman correlation was used to test the correlation of features with conventional quantitative metrics such as SUV, metabolic tumour volume, and total lesion glycolysis. Specificity and sensitivity (including 95% confidence intervals [CI]) for each of the studied parameters were derived using receiver operative characteristic (ROC) curves. Univariate and multivariate analyses were used to identify independent predictors associated with BMI.

Results: Correlation between conventional PET metrics and features ranged between 0.50 and 0.97 for positive correlation (33 significant association features) and ranged from –0.52 to –0.97 for inverse correlation (three significant association features) for both strong and moderate correlations. Analysis of ROC curves showed that high-intensity long-run emphasis 4 bin, high-intensity large zone emphasis 64 bin, long-run emphasis (LRE) 64 bin, large-zone emphasis 64 bin, max spectrum 8 bin, busyness 64 bin, and code similarity 32 and 64 bin were significant discriminators of BMI among other features (area under curve > 0.682, p < 0.05). Univariate analyses of texture features showed that code similarity and long-run emphasis (both 64 bin) were significant predictors of bone marrow involvement. Multivariate analyses revealed that LRE (64 bin, p = 0.031) with an odds ratio of 1.022 and 95% CI of (1.002–1.043) were independent variables for bone marrow involvement.

Conclusions: 18F-FDG PET/CT radiomic features are synergistic to visual assessment of BMI in patients diagnosed with lymphoma using 18F-FDG PET/CT. Further assessment of long-run emphasis is highly warranted.

Key words: bone marrow, texture analysis, 18F-FDG PET/CT, radiomics.

Introduction

Metabolic imaging using fluorine-18-fluorodeoxyglucose (18F-FDG) positron emission tomography (PET) with integrated computed tomography (CT) (18F-FDG PET/CT) is now the standard of care in clinical oncology. It has been used successfully for staging, restaging, patient stratification, and treatment response planning and prediction [1,2]. Lymphoma is a heterogeneous type of disease that arises from the constituent cells of the immune system or from their precursors that arise in lymph nodes

close to any organ or tissue in the body. Therefore, all organ systems may be involved at some stage of the disease including the central nervous system, head and neck, thorax, abdomen, gonads, bone, and others [3,4].

CT is the most often used imaging modality for staging malignant lymphoma due to its excellent availability and relatively low cost [5], but sometimes CT impedes identification of disease in normal-sized organs and detection of lesions that have poor contrast with the surrounding tissues. Another reason is that CT is not effective in diagnosis lymphoma with less reliability. It can detect bone marrow infiltration (BMI) in the late stage of the disease [6].

PET/CT has been validated to assess patients with different types of malignant tumours, including lymphomas, despite its relatively high cost [7]. The incidence of marrow disease varies with the histological subtype of lymphoma. Bone marrow biopsy is fundamental in identifying marrow involvement for therapy purposes [8]. Marrow diseases can be diagnosed with 18F-FDG PET/CT scan and the visual interpretation of marrow features of FDG uptake throughout the whole body. PET scans can efficiently determine

marrow disease status in a high proportion of lymphoma patients. Therefore, PET has the potential to reduce the guide for staging marrow biopsy [9]. However, interobserver variability remains a limiting factor in qualitative image analysis.

The sensitivity of FDG PET scan is similar to bone marrow biopsy (pathological sample) that confirms that PET scan is essential during the staging of lymphomas [10,11]. This result, if confirmed, will provide two identical methods for diagnosis of lymphomas. However, the use of 18F-FDG PET/CT in the sole assessment of the bone marrow and whether it can replace bone marrow biopsy is still controversial, and thus investigation with PET/CT scan through image analysis is potentially advised [5]. However, it could be useful to strengthen the diagnostic power of PET imaging through sophisticated data analysis using the diverse capabilities of PET texture analysis.

The aim of this study was to explore whether the textural features are able to provide diagnostic information of BMI in patients with lymphoma using 18F-FDG PET/CT.

Material and methods

Patients

Forty-four patients (43.2, 56.8% male) who were diagnosed with lymphoma were retrospectively retrieved from our data records. The retrospective nature of the study obviated the need to ask for patient consent. Ethical approval was obtained to perform the study. The inclusion criteria were those patients who had not had prior treatment before initial 18F-FDG diagnosis. Bone marrow involvement were confirmed by two clinical observers who have 5 and 10 years of experience in reading and interpretation of 18F-FDG PET/CT. The number of patients who had BMI was 18 (41%), as agreed by the two observers. Patients' demographics and characteristics are combined and summarised in Table 1.

Fluorine-18-fluorodeoxyglucose positron emission tomography computed tomography image acquisition

Patients fasted for six hours and had serum glucose concentration < 200 mg/dl before the intravenous injection of 185-370 MBq of 18F-FDG (0.1 mCi/kg of body weight). 18F-FDG PET/CT was performed using a Gemini 64 LXL PT/CT scanner (Philips Healthcare) in seven patients, whereas in five patients it was performed on a Gemini 64 TF TOF PT/CT (Philips Healthcare). The remaining 32 patients were imaged on a Biograph 20 mCT scanner (Siemens Medical Solutions).

During the imaging process, patients were in supine position with both arms extended in the cranial direction and breathing quietly. PET images were obtained at 2 min/bed frame for patients less than 60 kg, 2.5 min/bed frame for patients less than 90 kg, and 3 min/bed frame

Table 1. Clinical characteristics and acquisition parameters of the study population

Parameter	
Sex, *n*	
Male	25
Female	19
Age, years	
Median	47
Range	19-88
Bone marrow invasion by PET, *n*	
Yes	18
No	26
Blood glucose, mg/dl	
Median	102.5
Range	70-135
Weight, kg	
Median	73.5
Range	50-110
Injected radioactivity (18F-FDG), MBq	
Median	277.5
Range	185-370
18F-FDG uptake time, min	
Median	55
Range	50-60
Time per bed position, min	2-3
Scan time range, min	16-27

18F-FDG – fluorine-18-fluorodeoxyglucose, PET – positron emission tomography

for patents up to 90 kg. PET images were reconstructed using CT-based attenuation correction by an ordered-subset expectation maximisation iterative reconstruction algorithm with a slice thickness of 3 mm, and a pitch of 4 mm for the Biograph mCT, and slice thickness of 4 mm and a pitch of 4 mm for both imaging systems.

Radiomics extraction and features analysis

All images were transferred to a personal computer that contained Chang-Gung Image Texture Analysis (CGITA) toolbox version 1.4. PET images were then imported into the CGITA toolbox. CGITA is an open-source software code with a graphic user interface for texture analysis running on MATLAB (Math Works Inc., version 2015a) [12]. PET images were manually or semi-automatically contoured with an iso-contour threshold that was set to an absolute standardised uptake value (SUV) value of 3.0, as previously described [13]. All scans were analysed by senior residents independently (more than five years of experience) and were interpreted by a senior radiologist (10 years of experience).

The second step consisted of resampling or interpolating the non-cubic voxel grids into cubic voxels (2 mm) and performing quantisation (also called discretisation, down sampling, or resampling) of the original intensities into a discrete set of values between the minimum and maximum within the volume of interest (VOI). This number determines the size of the matrices from which the different texture features will be subsequently calculated. Bin numbers of 4, 8, 16, 32, and 64 were employed in this study. The third step comprised the extraction of a total of 73 radiomics parameters from images, including texture features and conventional PET metrics such as SUV_{max}, SUV_{mean}, SUV_{peak}, and total lesion glycolysis (TLG) for each VOI. SUV_{peak} was defined as the mean SUV within a 1-cm sphere centred on the maximum pixel [14].

Texture analysis

Texture analysis includes first-, second-, and higher-order texture methods as well as various transform-based methods. The most "direct" features were those based simply on intensity values within a region of interest (ROI). Texture features in the lymphoma are based on the same parent matrices that were utilised in tumour sites. Examples of these include the grey-level co-occurrence matrix (GLCM), the grey level run length matrix (GLRLM), the neighbourhood intensity difference matrix (NIDM), neighbourhood grey-level dependence matrix (NGLDM), and the intensity size-zone matrix (ISZM) [15–17].

The derived features from voxels of the segmented PET images were grouped into different categories. First-order features were derived from the histogram of voxel intensities (SUV_{mean}, SUV_{max}, skewness, kurtosis, etc.). Second-order textural features were based on matrices that

contained information about the regional spatial arrangement of the voxels, such as their homogeneity, contrast, and coarseness, simulating the human perception of the image. Higher-order features such as grey-level run-length features focused on local collinear voxels with the same grey level. Table 2 describes the extracted features using the CGITA toolbox from the segmented images.

Statistical analysis

Spearman correlation coefficient (rho) was used to evaluate the pairwise relationships between SUV_{mean}, SUV_{max},

Table 2. Spearman correlation between texture features and the most commonly used positron emission tomography quantitative metrics. The table shows variable degree of associations being highest and strong correlation coefficient

Strong correlation					
Variable	Correlation coefficient (Spearman's rho, ρ)				
	TLG				
	4	8	16	32	64
Contrast	0.829	0.855	0.854	0.854	0.855
Entropy	−0.798	−0.798	−0.780	−0.763	−0.727
Homogeneity	0.790	0.784	0.754	0.731	0.701
Dissimilarity	0.825	0.847	0.849	0.848	0.852
Inverse difference moment	0.790	0.779	0.732	0.707	0.702
Tumour volume	0.792	0.792	0.789	0.796	0.792
Surface area					
A sphericity	0.798	0.798	0.797	0.793	0.798
MTV					
Contrast	0.859	0.849	0.813	0.801	0.795
Entropy	−0.967	−0.969	−0.969	−0.969	−0.946
Homogeneity	0.970	0.969	0.961	0.950	0.909
Dissimilarity	0.862	0.892	0.893	0.887	0.888
Inverse difference moment	0.970	0.969	0.954	0.920	0.827
Intensity variability	0.754	0.742	0.751	0.772	0.748
Run-length variability	0.839	0.883	0.865	0.844	0.811
TLG	0.792	0.792	0.789	0.796	0.792
SUV_{mean}					
Minimum SUV	0.731	0.731	0.736	0.704	0.731
Maximum SUV	0.801	0.801	0.811	0.756	0.801
SUV SD	0.865	0.865	0.870	0.850	0.865
SUV_{max}					
Mean SUV	0.801	0.801	0.811	0.756	0.801
SUV Variance	0.836	0.836	0.796	0.876	0.836
SUV SD	0.930	0.930	0.932	0.929	0.930

TLG – total lesion glycolysis, MTV – metabolic tumour volume, SUV – standardised uptake value, SD – standard deviation

SUV_{peak}, TLG, surface area, and the derived 72 texture features including all bin sizes. Because not all the parameters contributed to differentiating lymphoma disease, we resorted to the results of the operation characteristic curve at each bin size, and to test the diagnostic potential of the quantitative indices including the conventional metrics as well as texture features, in the discrimination of bone marrow invasion (Table 2) [18,19]. Specificity and sensitivity (including 95% confidence intervals [CIs]) for each of the investigated parameters were also derived and calculated. The Youden index is the vertical distance between the 45-degree line and the point on the receiver operating characteristic (ROC) curve. Receiver operative characteristic data analysis was performed. Binary logistic regression test was used to express results of univariate then multivariate analysis for those features of high area under the curve (AUC) derived from ROC data plots. All statistical analysis was performed using SPSS software (IBM Corp, Armonk, New York, version 23). A p-value of < 0.05 was defined as statistically significant. No adjustment for multiple comparisons was made in this analysis.

Results

Correlation between conventional positron emission tomography metrics and texture features

The results of correlation of PET texture indices with the conventional quantitative metrics, namely maximum SUV (SUV_{max}), mean SUV (SUV_{mean}), TLG, metabolic tumour volume (MTV), SUV_{peak}, and surface area, are summarised in Tables 2 and 3. A general observation was that texture features obtained from all analysed bin sizes showed a moderate to strong correlation with conventional PET metrics. Spearman's rank correlation coefficients (rho) ranged from 0.50 to 0.97 for positive correlation and from −0.52 to −0.97 for the inverse correlation.

Receiver operative characteristic curves

The area under curve from ROC analysis was determined for every texture index. Out of the complete 73 textural features derived from CGITA, it was found that eight textural features had AUC significantly higher than 0.6 ($p < 0.05$) for bin sizes 4, 8, 32, and 64, while data derived from 16 bin did not contain any significant results. Table 4 describes the texture features that showed significant AUC higher than 0.6 ($p < 0.05$). Receiver operating characteristic curves of the significant data are shown in Figure 1. For all significant data, the code similarity had a higher AUC, with sensitivity of 55.6 and 50% and specificity of 84.6 and 88.5% for 32 and 64 bin, respectively.

Univariate and multivariate binary logistic regression

Univariate and multivariate binary logistic regression (UVA and MVA) analysis was performed for the features of high AUC derived from ROC data plots, and the results are shown in Table 5. In univariate binary logistic analysis two textural features showed statistically significant association with bone infiltration, whereas multivariate analysis yielded one texture feature (long-run emphasis [LRE] 64 bin, $p = 0.031$; odds ratio 1.022; 95% CI = 1.002–1.043) that showed statistically significant association with bone infiltration. The set of variables in the MVA included all the significant variables in the univariate setting, using the forward likelihood method.

Discussion

Quantitative features are descriptors extracted from the images using computational mathematical algorithms. The extracted features from PET/CT images using different matrices include GLCM, GLRLM, NIDM, NGLDM, and ISZM [12,20].

Table 3. Spearman correlation between texture features and the most commonly used positron emission tomography quantitative metrics. The table shows variable degree of associations being higher and moderate correlation coefficient

Moderate correlation					
Variable	**Correlation coefficient (Spearman's rho, ρ)**				
	TLG				
	4	**8**	**16**	**32**	**64**
Intensity variability	0.529	0.519	0.530	0.565	0.581
Run-length variability	0.632	0.700	0.677	0.670	0.681
Maximum SUV	0.530	0.530	0.528	0.527	0.530
Mean SUV	0.502	0.502	0.500	0.502	0.502
SUV variance	0.583	0.583	0.579	0.587	0.583
SUV SD	0.582	0.582	0.546	0.590	0.582
Surface area					
Entropy	−0.526	−0.531	−0.520	−0.553	−0.543
Homogeneity	0.543	0.545	0.527	0.560	0.539
Inverse difference moment	0.543	0.547	0.531	0.557	0.504
Tumour volume	0.635	0.635	0.627	0.641	0.635
MTV					
Long-run emphasis	0.5	0.501	0.588	0.672	0.634
Low-intensity long-run emphasis	0.5	0.503	0.593	0.677	0.636
Surface area	0.635	0.635	0.627	0.641	0.635
SUV_{mean}					
SUV variance	0.655	0.655	0.636	0.653	0.655
TLG	0.502	0.502	0.501	0.502	0.502
SUV_{max}					
TLG	0.530	0.530	0.525	0.527	0.530

TLG – total lesion glycolysis, SUV – standardised uptake value, MTV – metabolic tumour volume
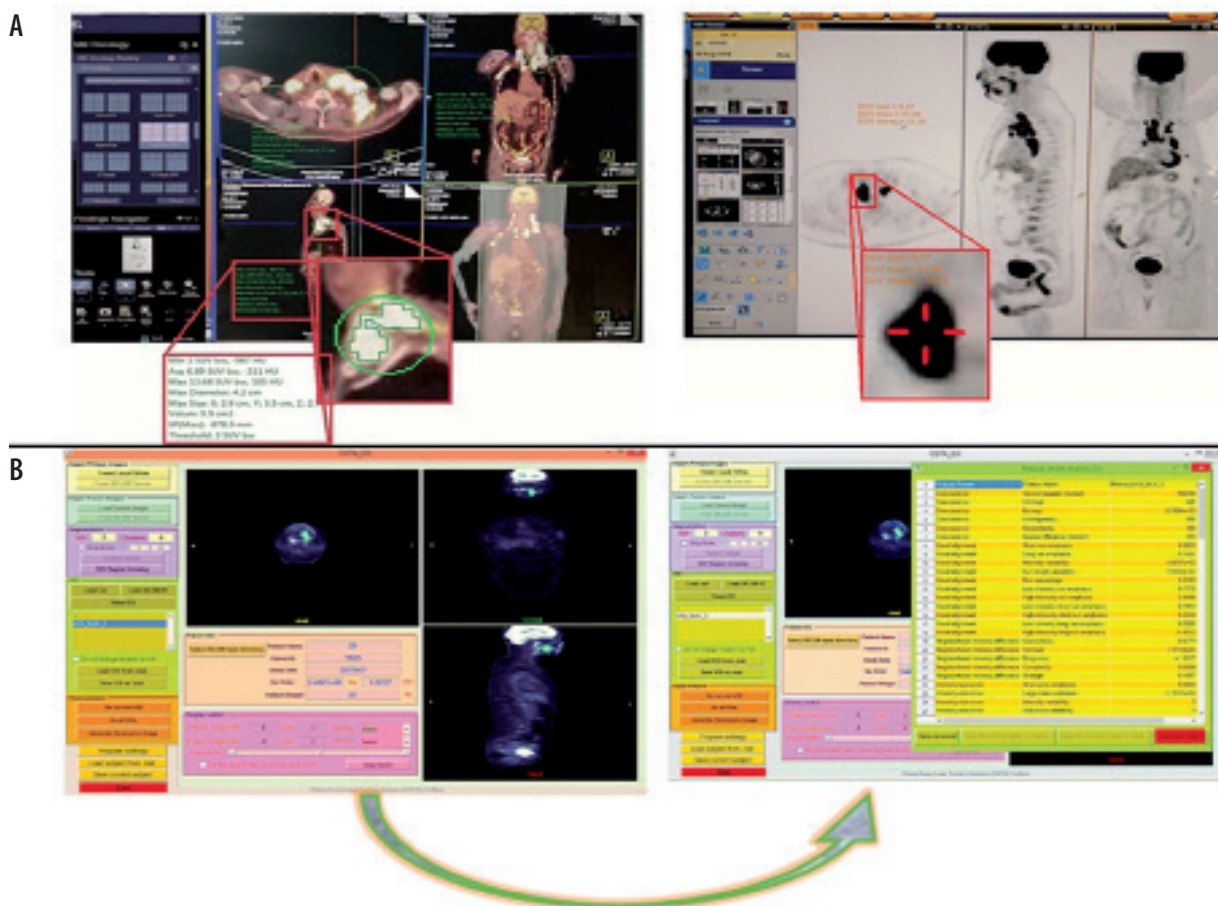
Figure 1. A) The figures describe traditional standardised uptake value (SUV) measurements through different positron emission tomography–computed tomography (PET/CT) workstation and (**B**) figures describe steps of features extraction through Chang-Gung Image Texture Analysis (CGITA) package code depending on given SUV. The CGITA GUI provides users with a simple image display interface that allows users to examine different slices and views. The computation of heterogeneity indices is achieved simply by button clicking. The current functions and interfaces of CGITA can be customized by users familiar with MATLAB programming. The screen shot here shows a subject with the ^{18}F-FDG-PET images

Table 4. Area under curve results of receiver operating characteristics demonstrated for those parameters that showed a statistically significant area greater than 0.5

Bin size	Variable	AUC	Sig.	Sens.	Spec.	Criterion	Lower bound	Upper bound
4	High-intensity long-run emphasis	0.739	0.008	66.7	76.9	> 74.23	0.587	0.891
8	Max spectrum	0.682	0.042	44.4	88.5	> 0.126	0.522	0.842
32	Code similarity	0.714	0.017	55.6	84.6	≤ 0.005	0.553	0.874
64	Long-run emphasis	0.709	0.019	61.1	76.9	> 39.36	0.554	0.865
	Busyness	0.705	0.022	77.8	65.4	> 2.262	0.535	0.875
	Large-zone emphasis	0.701	0.025	61.1	76.9	> 99688.3	0.541	0.861
	High-intensity large-zone emphasis	0.718	0.015	55.6	84.6	> 140111.2	0.563	0.873
	Code similarity	0.707	0.021	50	88.5	≤ 0.008	0.548	0.867

AUC – area under curve

^{18}F-FDG PET\CT plays an important role in diagnosis, staging, treatment monitoring, prognosis, and assessment of lymphoma [21]. Also, a heterogeneity metric can only have complementary (or higher significant association) value if it is not highly correlated with the corresponding volume [22]. The correlation between heterogeneity metrics and the conventional PET indices showed significant association for 21 parameters (rho ≥ 0.7) with strong correlation and 16 parameters with moderate correlation (0.7 > rho ≥ 0.5).

The hypothesis of this study was to find a correlation between tumour texture heterogeneity as revealed by radiomics analysis of primary lymphomatous lesion and bone marrow involvement. The use of texture features in

Table 5. Univariate and multivariate binary logistic regression analysis performed for those features of high area under curve derived from receiver operating characteristics data plots

Univariate analysis			
Risk factors	**Odds ratio**	**(95% CI)**	**p-value**
High-intensity long-run emphasis (4 bin)	1.010	(0.991-1.023)	0.102
Max spectrum (8 bin)	28.45	(0.32-2525.05)	0.143
Code Similarity (32 bin)	1.000	(1.000-1.000)	0.100
Long-run emphasis (64 bin)	1.021	(1.000-1.043)	0.025*
Busyness (64 bin)	1.011	(0.971-1.052)	0.590
Large-zone emphasis (64 bin)	1.000	(1.000-1.000)	0.362
High-intensity large-zone emphasis (64 bin)	1.000	(1.000-1.000)	0.340
Code Similarity (64 bin)	1.000	(1.000-1.000)	0.039*
Multivariate analysis			
Long-run emphasis (64 bin)	1.022	(1.002-1.043)	0.031*

* Significant at type I error of 5% CI = confidence interval.

differentiating between tumour cells of low or high metastatic spread could be a key tool in bone marrow involvement or at least serve as an adjunct in improving the diagnostic performance of ¹⁸F-FDG PET/CT in the staging and management of lymphoma patients.

Bone marrow biopsy has been the conventional method of assessment of BMI. It has several staging, treatment, and prognostic implications [23]. Limitations of bone marrow biopsy include site-dependence and discordance in morphology between lymphomatous cells in extramedullary sites and those cells in the bone marrow [24]. In addition, histological data may report a different pathologic non-lymphoma-related malignancy or disorder as well as its invasive nature, pain, and clinician expertise.

Other drawbacks include extra medical staff, sample fixation, and decalcification as well as a longer stay in the clinic. No more likely but also adding some burden to the examination is the addition of trephine biopsy with bone marrow aspiration, which may cause some adverse events including haemorrhage and morbidity [25]. Another major shortcoming is the likelihood of missing focal disease because the biopsy normally does not cover the entire portion of bone marrow. These shortcomings of bone marrow biopsy stimulate the search for alternative methods that might obviate the need for such procedures whilst being able to provide at least equivalent if not better diagnostic performance.

However, ¹⁸F-FDG PET/CT has several advantages in this context, including full body coverage, less invasiveness, precise local assessment of diffuse vs. focal infiltration using anatomical features, as well as the possibility of quantitative data interpretation. The current study focuses on the latter advantage using not only the conventional PET metrics but also incorporating the new advances in texture feature analysis and radiomics data extraction.

The replacement of ¹⁸F-FDG PET/CT to bone marrow biopsy is still a matter of active debate. However, the quantitative capacity and recent advances in radiomics data analysis open up new avenues in this context. The present paper aimed to find a major PET feature that could be utilised in future studies as a benchmark or evident source in eliciting more biological characteristics of bone marrow invasion.

Several researches have confirmed a relationship between greater FDG uptake and more aggressive course of malignancy in lymphoma [26,27]. The resulting significant features confirmed that ¹⁸F-FDG PET images have advantages of combining practical and anatomical information, which is regarded as a popular contemporary reference for the management of lymphomas [28]. In another study, when looking into the prognostic performance of the texture data, MTV was found the most statistically significant parameter that shoed the largest correlation coefficient [22]. A recent report looking at the differences that arise from tumour volume segmentation has shown that low MTV had a significantly longer progression-free survival and overall survival compared to patients with high MTV. These findings were obtained regardless of the segmentation methods used [29].

The conventional PET indices depend on radioactivity concentration measured by the PET scanner within a region of interest (ROI) (¹⁸F-FDG uptake interior contoured lesion) [30], while biopsy (i.e. pathological sample) is the gold standard for determining tumour genetics [31]. However, genomic features of gene expression and pathways can be predicted by FDG uptake features from the lesion [32]. Therefore, the correlation between conventional matrix (such as SUV_{mean}, SUV_{max}, TLG) and quantitative features from PET images (especially those with strong correlation) can be considered as an acceptable surrogate to replace those features instead of guided biopsy, to prevent delayed diagnosis and the other associated complications described earlier.

While ROC analysis could provide a static assessment of risk identification through cut-off points that maximise sensitivity and specificity, it can also provide important information about diagnostic test performance [33,34]. In this work, the event in the ROC curve depends on the presence or absence of BMI for each individual patient. By comparing AUC of ROC curves of texture parameters, we found that texture parameters could have strong discriminating capabilities in identifying patients who have BMI This effective diagnostic capacity was statistically absent in the conventional and standard method of quantitation including SUV_{max}, SUV_{mean}, SUV_{peaks}, TLG, and MTV.

For texture feature investigated in the present study, high-intensity large run emphasis (HILRE) achieved the highest AUC (0.718, CI: 0.563-0.873) among all significant data of ROC curves. Long-run emphasis, however, has a significant strong correlation with metabolic volume, which might underscore its performance in bone marrow involvement.

¹⁸F-FDG PET/CT has been widely used for lymphoma diagnosis because the specificity and sensitivity have higher
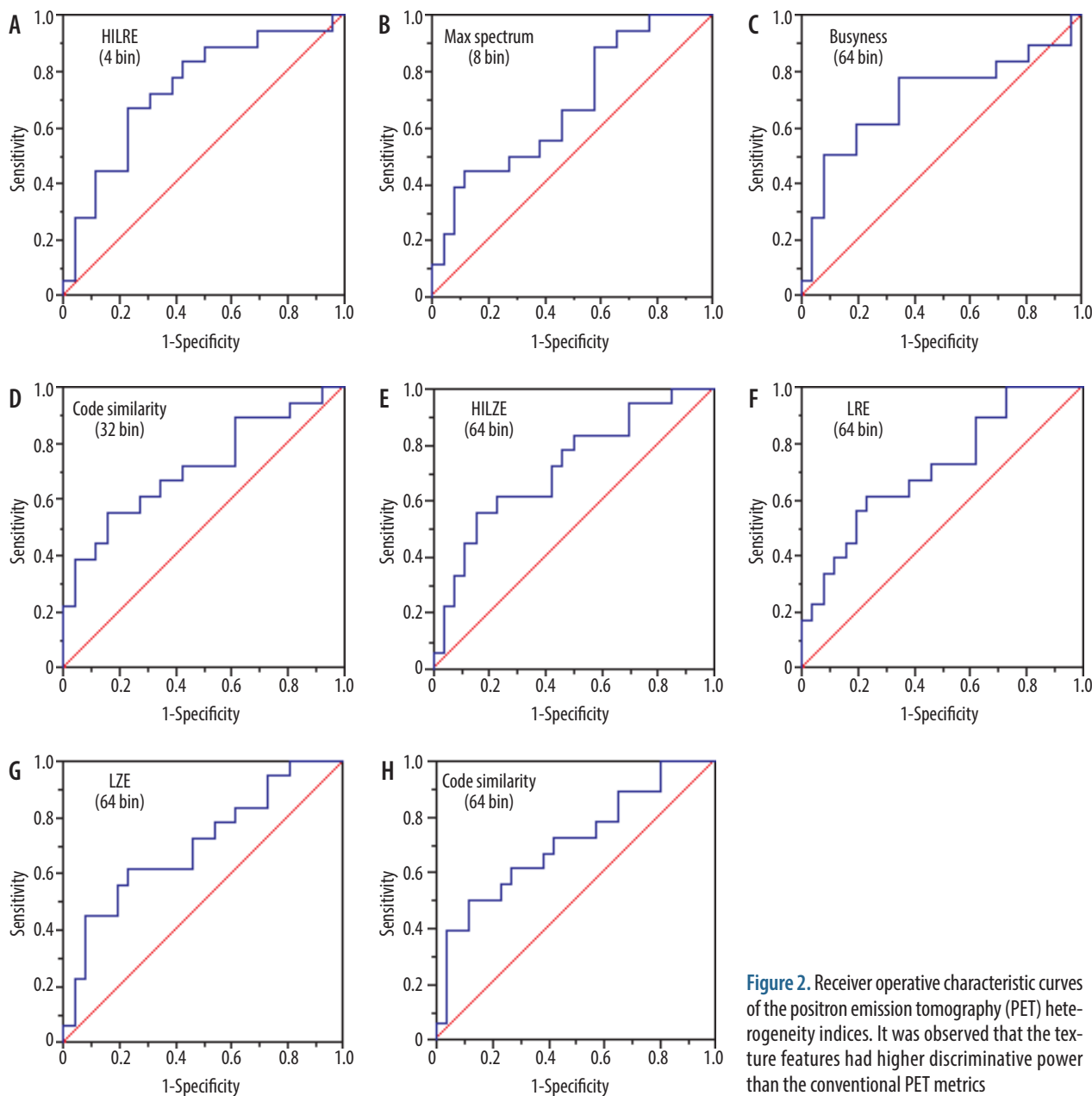
Figure 2. Receiver operative characteristic curves of the positron emission tomography (PET) heterogeneity indices. It was observed that the texture features had higher discriminative power than the conventional PET metrics

indications in lymphoma regions, especially in the initial staging procedures [11,35]. In fact, second-order and high-order statistics (i.e. based on grey-level matrix, nearest neighbour spatial dependence matrices, voxel-alignment matrix, intensity size-zone matrix, texture feature coding co-occurrence matrix, etc.) provide information from the spatial relationship of image voxels. Moreover, a multitude of features may be derived from the grey-level matrices to characterise the structure of interest [36]. These features are independent of tumour position, orientation, size, and brightness and |consider the local intensity-spatial distribution [37].

Based on the ROC curves, the results showed that HILRE (4 bin) long-run emphasis (LRE 64 bin) (i.e. voxel-alignment matrix [38]), high-intensity large-zone emphasis 64 bin, large-zone emphasis (large zone emphasis 64 bin) (i.e. intensity size-zone matrix [39]), max spectrum (8 bin) (i.e. spectrum matrix) [40], busyness (64 bin) (neighbour-

hood grey intensity difference matrix [41]), and code similarity (32 bin and 64 bin) (coding co-occurrence matrix [42]) were significant predictors of BMI ($p < 0.05$). These features were extracted from the second- and higher-order matrix, highlighting the relevance of voxel arrangement and their spatial correlation to the underlying biological processes of BMI. To our knowledge, this finding has not been reported in the literature.

Busyness extracted from contoured PET images offered a greater discriminatory power marked by higher accuracy, specificity, and sensitivity than commonly used quantitative metrics such as SUV_{max}, which was not significant in this study. It has been reported that the NGIDM texture features were able to differentiate malignant pulmonary nodules [43]. The enhancement in discriminatory performance shown in this study could benefit patients by preventing the high false-positive rate of PET for FDG uptake regions.

One limitation of the present study was the pathological guidance of BMI in the selected patient cohort. This should be tackled in validation studies investigating the role of texture feature analysis in diagnosing BMI in lymphoma patients. Future studies are therefore highly warranted to confirm the performance of the texture data described herein, with special emphasis placed on code similarity and long-run emphasis.

Conclusions

In conclusion, our study confirmed the role of texture analysis and therefore proposed a new method for dif-ferentiating lymphoma disease with BMI. More investigations are highly warranted, to combine the role of texture analysis in providing additional diagnostic as well as prognostic values to ^{18}F-FDG PET/CT in the initial staging of patients with lymphoma.

Conflict of interest

The authors report no conflict of interest.

References

1. Moskowitz CH, Schoder H, Teruya-Feldstein J, et al. Risk-adapted dose-dense immunochemotherapy determined by interim FDG-PET in Advanced-stage diffuse large B-Cell lymphoma. J Clin Oncol 2010; 28: 1896-1903.

2. Minamimoto R, Fayad L, Advani R, et al. Diffuse large B-Cell lymphoma: prospective multicenter comparison of early interim FLT PET/CT versus FDG PET/CT with IHP, EORTC, deauville, and PERCIST criteria for early therapeutic monitoring. Radiology 2016; 280: 220-229.

3. D'Souza MM, Jaimini A, Bansal A, et al. FDG-PET/CT in lymphoma. Indian J Radiol Imaging 2013; 23: 354-365.

4. Toma P, Granata C, Rossi A, et al. Multimodality imaging of Hodgkin disease and non-Hodgkin lymphomas in children. Radiographics 2007; 27: 1335-1354.

5. Armitage JO. Staging non-Hodgkin lymphoma. Cancer J Clin 2005; 55: 368-376.

6. Vinnicombe SJ, Reznek RH. Computerised tomography in the staging of Hodgkin's disease and non-Hodgkin's lymphoma. Eur J Nucl Med Mol Imaging 2003; 30: S42-55.

7. Buchpiguel CA. Current status of PET/CT in the diagnosis and follow up of lymphomas. Rev Bras Hematol Hemoter 2011; 33: 140-147.

8. Weber AL, Rahemtullah A, Ferry JA. Hodgkin and non-Hodgkin lymphoma of the head and neck: clinical, pathologic, and imaging evaluation. Neuroimaging Clin N Am 2003; 13: 371-392.

9. Carr R, Barrington S, Madan B, et al. Detection of lymphoma in bone marrow by whole-body positron emission tomography. Blood 1998; 91: 3340-3346.

10. Pelosi E, Penna D, Douroukas A, et al. Bone marrow disease detection with FDG-PET/CT and bone marrow biopsy during the staging of malignant lymphoma: results from a large multicentre study. Q J Nucl Med Mol Imaging 2011, 55: 469-475.

11. Paes FM, Kalkanis DG, Sideras PA, et al. FDG PET/CT of extranodal involvement in non-Hodgkin lymphoma and Hodgkin disease. Radiographics 2010; 30: 269-291.

12. Fang YH, Lin CY, Shih MJ, et al. Development and evaluation of an open-source software package "CGITA" for quantifying tumor heterogeneity with molecular images. Biomed Res Int 2014; 2014: 248505.

13. Cheng NM, Fang YH, Chang JT, et al. Textural features of pretreatment 18F-FDG PET/CT images: prognostic significance in patients with advanced T-stage oropharyngeal squamous cell carcinoma. J Nucl Med 2013; 54: 1703-1709.

14. Wahl RL, Jacene H, Kasamon Y, et al. From RECIST to PERCIST: evolving considerations for PET response criteria in solid tumors. J Nucl Med 2009; 50: 122s-150s.

15. Castellano G, Bonilha L, Li LM, et al. Texture analysis of medical images. Clin Radiol 2004; 59: 1061-1069.

16. Soh LK, Tsatsoulis C. Texture analysis of SAR sea ice imagery using gray level co-occurrence matrices. IEEE Trans Geosci Remote Sensing 1999; 37: 780-795.

17. Lam SW. Texture feature extraction using gray level gradient based co-occurence matrices. In: 1996 IEEE International Conference on Systems, Man and Cybernetics Information Intelligence and Systems (Cat No96CH35929) 1996; 1996: 267-271.

18. Sultan S, Baloch N, Ahmed ZA, et al. Pattern of bone marrow involvement in non Hodgkin's lymphoma classified according to WHO classification: report of a developing country Pakistan. J Lab Physicians 2018; 10: 17-20.

19. Xu H, Guo W, Cui X, et al. three-dimensional texture analysis based on PET/CT images to distinguish hepatocellular carcinoma and hepatic lymphoma. Front Oncol 2019; 9: 844-844.

20. Larue R, van Timmeren JE, de Jong EEC, et al. Influence of gray level discretization on radiomic feature stability for different CT scanners, tube currents and slice thicknesses: a comprehensive phantom study. Acta Oncol 2017; 56: 1544-1553.

21. Chen Y, Zhou M, Liu J, et al. Prognostic value of bone marrow fdg uptake pattern of PET/CT in newly diagnosed diffuse large b-cell lymphoma. J Cancer 2018; 9: 1231-1238.

22. Hatt M, Tixier F, Pierce L, et al. Characterization of PET/CT images using texture analysis: the past, the present... any future? Eur J Nucl Med Mol Imaging 2017; 44: 151-165.

23. Adams HJ, Nievelstein RA, Kwee TC. Opportunities and limitations of bone marrow biopsy and bone marrow FDG-PET in lymphoma. Blood Rev 2015; 29: 417-425.

24. Arber DA, George TI. Bone marrow biopsy involvement by non-Hodgkin's lymphoma: frequency of lymphoma types, patterns,

blood involvement, and discordance with other sites in 450 specimens. Am J Surg Pathol 2005; 29: 1549-1557.

25. Bain BJ. Morbidity associated with bone marrow aspiration and trephine biopsy – a review of UK data for 2004. Haematologica 2006; 91: 1293-1294.

26. Schoder H, Noy A, Gonen M, et al. Intensity of 18fluorodeoxyglucose uptake in positron emission tomography distinguishes between indolent and aggressive non-Hodgkin's lymphoma. J Clin Oncol 2005; 23: 4643-4651.

27. Wu X, Pertovaara H, Korkola P, et al. Correlations between functional imaging markers derived from PET/CT and diffusion-weighted MRI in diffuse large B-cell lymphoma and follicular lymphoma. PLoS One 2014; 9: e84999-e84999.

28. Okada M, Sato N, Ishii K, et al. FDG PET/CT versus CT, MR imaging, and 67Ga scintigraphy in the posttherapy evaluation of malignant lymphoma. Radiographics 2010; 30: 939-957.

29. Ceriani L, Milan L, Johnson PWM, et al. Baseline PET features to predict prognosis in primary mediastinal B cell lymphoma: a comparative analysis of different methods for measuring baseline metabolic tumour volume. Eur J Nucl Med Mol Imaging 2019; 46: 1334-1344.

30. Lucignani G, Paganelli G, Bombardieri E. The use of standardized uptake values for assessing FDG uptake with PET in oncology: a clinical perspective. Nucl Med Communications 2004; 25: 651-656.

31. Moon SH, Kim J, Joung JG, et al. Correlations between metabolic texture features, genetic heterogeneity, and mutation burden in patients with lung cancer. Eur J Nucl Med Mol Imaging 2019; 46: 446-454.

32. Ahn KS, Kang KJ, Kim YH, et al. Genetic features associated with (18)F-FDG uptake in intrahepatic cholangiocarcinoma. Ann Surg Treat Res 2019; 96: 153-161.

33. Fan J, Upadhye S, Worster A. Understanding receiver operating characteristic (ROC) curves. CJEM 2006; 8: 19-20.

34. Kamarudin AN, Cox T, Kolamunnage-Dona R. Time-dependent ROC curve analysis in medical research: current methods and applications. BMC Med Res Methodol 2017; 17: 53-53.

35. Kwee TC, Kwee RM, Nievelstein RA. Imaging in staging of malignant lymphoma: a systematic review. Blood 2008; 111: 504-516.

36. El Naqa I, Grigsby P, Apte A, et al. Exploring feature-based approaches in PET images for predicting cancer treatment outcomes. Pattern Recognit 2009; 42: 1162-1171.

37. Greven KM. Positron-emission tomography for head and neck cancer. Semin Radiat Oncol 2004; 14: 121-129.

38. Loh H, Leu J, Luo RC. The analysis of natural textures using run length features. IEEE Trans Industrial Electron 1988; 35: 323-328.

39. Thibault G, Fertil B, Navarro C, et al. Texture indexes and gray level size zone matrix application to cell nuclei classification. Conference: 10th International Conference on Pattern Recognition and Information Processing 2009.

40. He DC, Wang L. Texture features based on texture spectrum. Pattern Rec 1991; 24: 391-399.

41. Amadasun M, King R. Textural features corresponding to textural properties. IEEE Trans Syst Man Cyber 1989; 19: 1264-1274.

42. Horng MH, Sun YN, Lin XZ. Texture feature coding method for classification of liver sonography. Comput Med Imaging Graph 2002; 26: 33-42.

43. Chen S, Harmon S, Perk T, et al. Using neighborhood gray tone difference matrix texture features on dual time point PET/CT images to differentiate malignant from benign FDG-avid solitary pulmonary nodules. Cancer Imaging 2019; 19: 56.